A 20 kW, 3-level flying capacitor 1500 V inverter with characterized GaN devices for grid-tie applications

Van Sang NGUYEN, Anthony BIER, Hajar ES-SEGHIER, Ulrich SOUPREMANIEN,
Gérard DELETTE, Stephane CATELLANI

CEA - French Alternative Energies and Atomic Energy Commission
50 avenue du Lac Léman
Le Bourget du Lac - 73375, France
Tel.: +33 / (0) 4 79 79 27 50
E-Mail: van-sang.nguyen@cea.fr
URL: www.cea.fr

Acknowledgements

The authors acknowledge CEA/LITEN - CARNOT project “FlyGaN” for funding the activities presented in this paper.

Keywords

«DC-AC converter», «Flying Capacitor Boost Converter», «Gallium Nitride (GaN)», «Photovoltaic» «Renewable energy systems»

Abstract

This work presents the static and dynamic characterizations of high voltage GaN power devices (GaN FET 900 V and GaN HEMT 1200 V) in order to implement a 3-level flying capacitor 1500 V_{DC} inverter for high power density grid-tie applications with renewable energy sources such as solar and hydrogen energy. In the first part, the static characterizations are shown for two selected GaN power devices. Then these GaN devices were placed in a double-pulse-test-bench dedicated to the dynamic characterizations intended to observe the switching behaviors of the devices under the nominal voltage and current. Finally, in order to demonstrate the compactness of the converter, these GaN devices were implemented in a 20 kW, 3-level flying capacitor 1500 V_{DC} inverter with the full-custom suitable passive elements of the output filters connected to the 800 V_{AC} 3-phase grid.

Introduction

Wide-band-gap power devices take an important place in the power electronics systems design. Today, SiC devices become mature and emerge in many high power electronics products [1]. On the other hand, lower voltages GaN devices ($\leq$ 650 V) are widely used for low power consumer applications, thanks to their efficient and compact designs [2]. Due to their thermal and blocking voltage constraints, GaN devices are still in optimizing stage for achieving high power applications, in particular, for 800 V 3-phase grid-tie applications with renewable energy power systems. Using 650 V GaN devices for applications with DC bus of 1500 V_{DC} requires the consideration of a high multi-level topology, where challenges are: the reliability, the control and the auxiliary circuitry of the systems [3]. Following up a recent work of the flying-capacitor topology on a SiC based design [4] and a GaN based design with a DC bus of 800 V_{DC} [5]; this article presents a design of a 3-level flying capacitor inverter working at 20 kW tied to the 800 V 3-phase grid where the nominal input voltage is 1500 V_{DC}. This GaN based design’s approach gives a potential compact solution to several renewable energy systems like solar, hydrogen or even battery power systems. Today’s trend in the large PV plant is the increasing in the power of the string by using smart panels [6]. Another work in parallel is ongoing where the GaN based power electronics parts are integrated inside the junction box of the PV panel, which allows installing

much more number of photovoltaic (PV) panels in a single string. In a conventional 1500 V string, the output power is typically at 10 kW, the power of the 1500 V smart string could excess 20 kW thanks to the higher number of the PV panels [6].

Working with 1500 V_{DC} bus voltage, GaN devices have to perform consequently with a nominal drain-source blocked voltage of 750 V in steady-state operations. This work analyses and challenges the GaN FET 900 V devices and the GaN HEMT 1200 V in such operating conditions. The comparison of these two GaN devices firstly takes place on a Keysight B1506A power device analyzer for the static characterizations, and then dynamic test-bench is used to qualify these selected GaN devices for estimating the switching losses under the nominal configurations. This article includes the design of the grid-filters inductors with thermal consideration and the simulations of this 1500 V inverter. Finally, this work shows the experimental results of this GaN based 3-level flying capacitor inverter until 20 kW characterizations.

High voltage GaN devices: static and dynamic characterizations

Static characterizations

By using a standard industrial test-bench (Keysight B1506A), the I/V curves, the threshold voltage and the parasitic capacitances of the selected GaN devices are extracted under the similar configurations. Fig. 1 shows large differences on the capacitance's characterization of DUT1 and DUT2 up to a drain-source voltage of 900 V. At this high voltage level, DUT1 has 958 pF of Ciss meanwhile this value of Ciss for DUT2 is 251 pF. A high frequency design up to a switching frequency of several MHz need to consider these capacitances; it is event more critical for the thermal issue in a high power design.

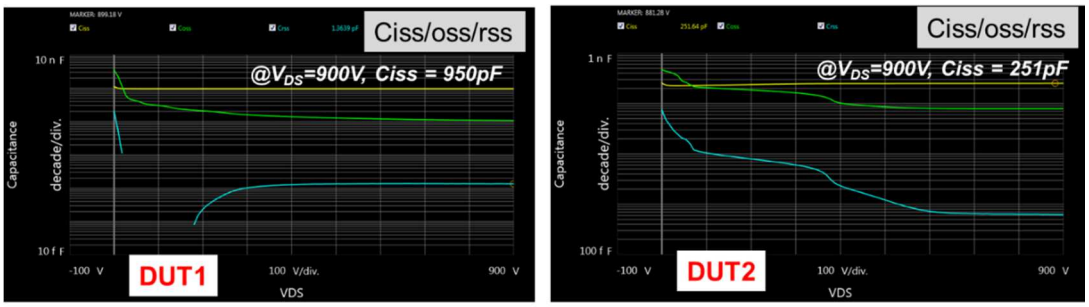

Fig. 1: Static characterizations of capacitances for GaN FET 900V (DUT1) and GaN HEMT 1200V (DUT2)

Under the similar configurations of the drain-source current, the threshold voltage of DUT1 is approximately 3.4 V and for DUT2 about 1.5 V. As well known, this value is extremely critical for GaN based high power applications where the transient voltage *dv/dt* is usually very high due to the high voltage applied on the devices. This *dv/dt* might be the main reason at the origin of short-circuit within an inverter-leg where there are complementary transistors located at high side and low side. Design of the grid-tie flying-capacitor inverter need to take into account carefully this issue due to the DC bus voltage of 1500 V.

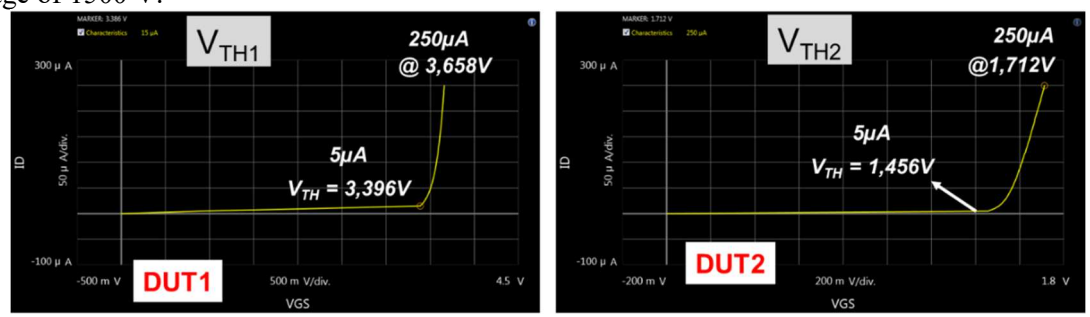

Fig. 2: Threshold voltages of GaN FET 900 V (DUT1) and GaN HEMT 1200 V (DUT2)

Fig. 3 and Fig. 4 show the static resistances and the current/voltage curves of these two GaN devices, the DUT1 has a higher capacitance; however, its resistance value is much smaller than the DUT2. These

static results suggest the correct driving voltage of each transistors in order to obtain the best performance of the devices.
Under a drain current (at 25°C) of 30 A with different driving voltages, the on-state resistance of DUT1 varies between 36 mΩ and 48 mΩ where the typical value on the datasheet is 50 mΩ. This value of second device (DUT2) under the similar conditions is comprised between 76 mΩ and 80 mΩ where the maximum static on-state resistance value in its preliminary datasheet is 75 mΩ.

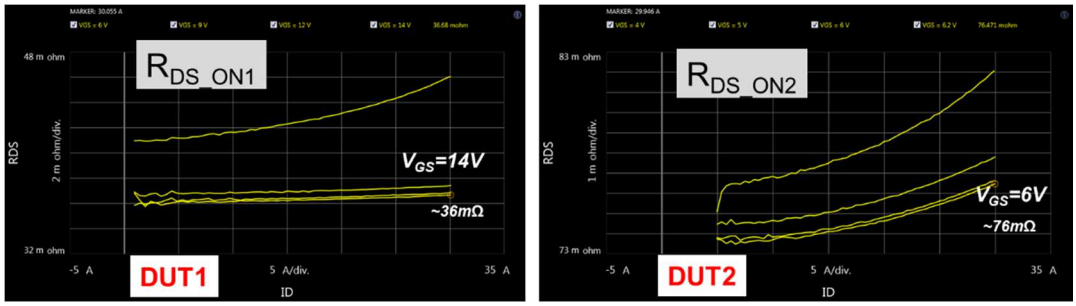

Fig. 3: Static resistances of GaN FET 900 V (DUT1) and GaN HEMT 1200 V (DUT2)

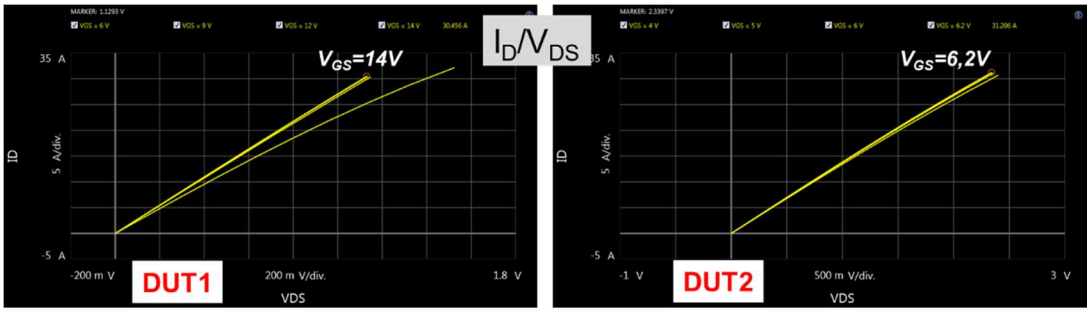

Fig. 4: Current/voltage characterizations of GaN FET 900 V (DUT1) and GaN HEMT 1200 V (DUT2)

Dynamic characterizations

After these static characterizations, the dynamic characterizations use the high bandwidth voltage and current probes [7], which are suitable for high-speed GaN devices. As in Fig. 5, an IZM current sensor with low insertion inductance of 0.3 nH and a bandwidth of 500 MHz [8] from Fraunhofer-IZM, [9] allows to record precisely the rising and falling edges of the drain-source current of the device. An IsoVU probe [8] with a bandwidth of 800 MHz is used to measure the drain-source voltage, a second low voltage probe with a bandwidth of 1 GHz measures the gate-source voltage.

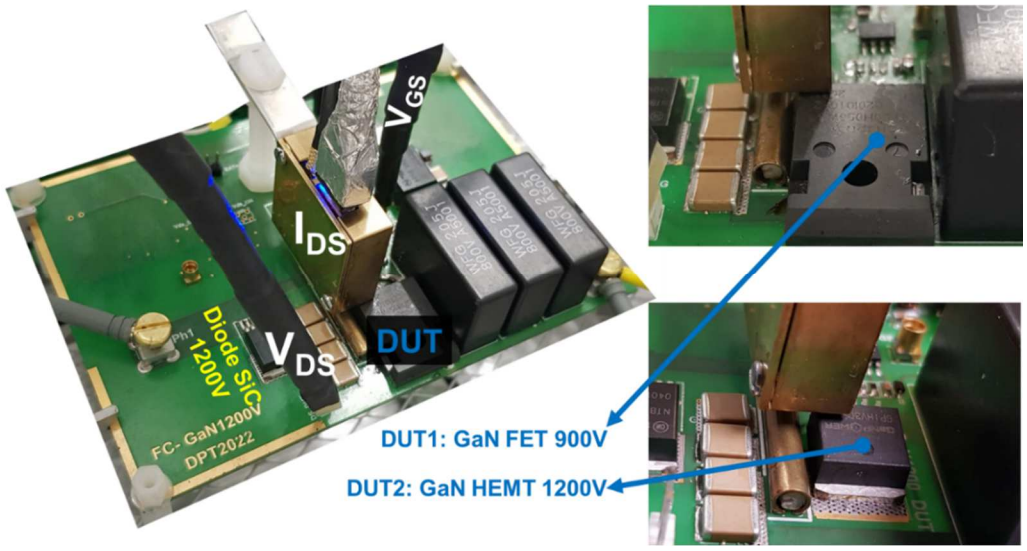

Fig. 5: Double-pulse-test bench with combined footprint for DUT1 and DUT2

From these measurements, the turn-on and turn-off losses can be calculated. During the experiments, difficulties were noticed to perform the dynamic characterization of DUT2 at the nominal voltage, we found out the problem on the gate driver. The set-up of the dynamic characterizations for DUT2 is ongoing. In this article, only experimental results of the dynamic characterizations on the DUT1 are presented.

Fig. 6 shows the experimental results of DUT1, which are the principal waveforms of the DPT set-up: the control signal on the gate V_{GS} of 0 V/9 V, the rising - falling edges from IZM sensor, the drain-source voltage V_{DS} of 0 V/760 V and the current on the inductance.

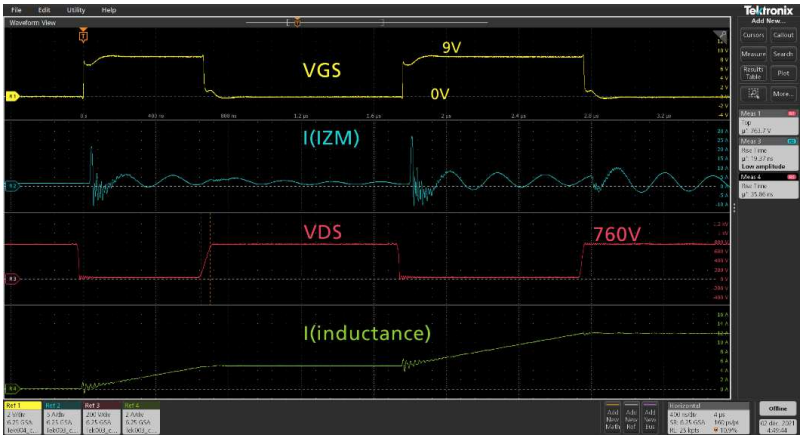

Fig. 6: Experimental waveforms of the DPT test

In Fig. 7, GaN devices (FET 900 V) turns on from a blocking voltage of 760 V, a peak slew rate *dv/dt* of 100 V/ns is observed.

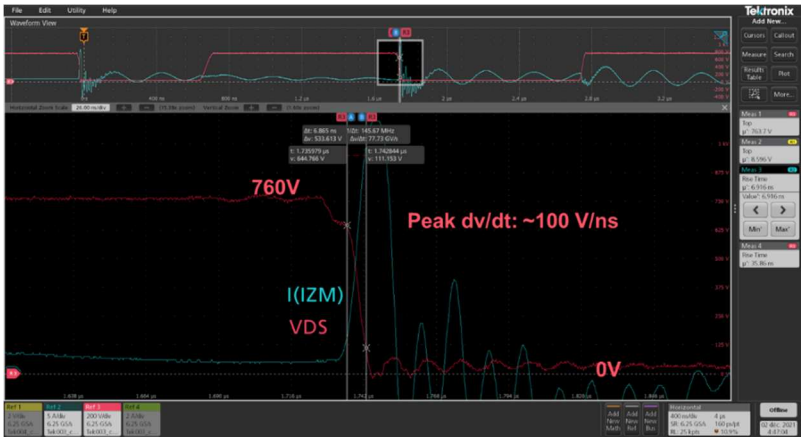

Fig. 7: Fall time of 6.8 ns of the drain source voltage (0 V/760 V) at turn-on

In Fig. 8, GaN FET 900 V devices turns off to block a voltage of 760 V, the peak slew rate *dv/dt* of 50 V/ns is observed in this rising edge.

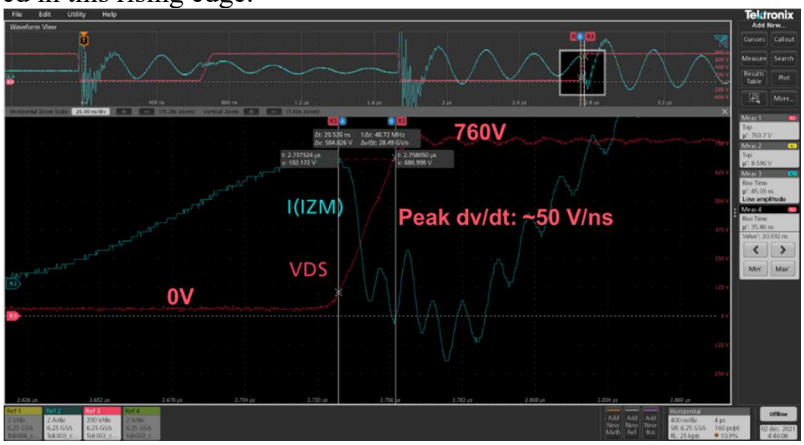

Fig. 8. Rise time of 20 ns of V_{DS} at turn-off

Simulations of the flying-capacitor 3-ph inverter

The electrical behavior of the 3-phase flying capacitor inverter is simulated using PLECS software. Fig. 9 shows a one-phase schematic representation model of the converter power stage. A 1500 V_{DC} voltage source is placed at the input and the inverter is connected to the 800 V_{AC} grid via a LCL-type filter. The current flowing through inductor L_1 is controlled within a PI-based control. The current control loop and the grid voltage synchronization is implemented considering the rotating reference frame (DQ domain).

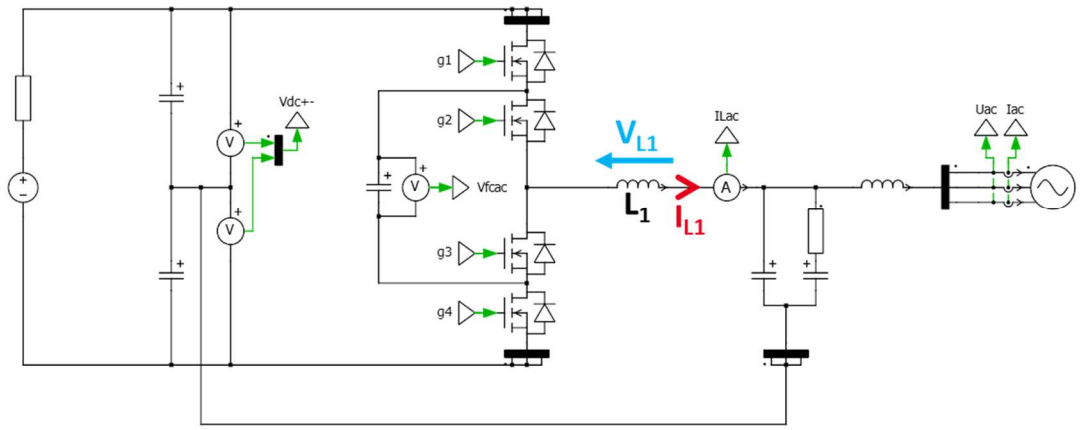

Fig. 9: PLECS simulation of the 3-phase flying-capacitor inverter

Simulation results are focused in Fig. 10 on the voltage and the current waveform of the inductor L_1.For a 20 kW 3-phase inverter, the peak value of the 50 Hz fundamental frequency sinusoidal AC current is 20 A and the RMS value of the signal 14.4 A. A 200 kHz triangular current ripple can be observed, which is twice the working frequency of the GaN devices. For the inductor design, its voltage must also be taken into account. The challenge in the design of the output filter, for a high power application, is the compliance to the high current, high voltage and high frequency at the same time.

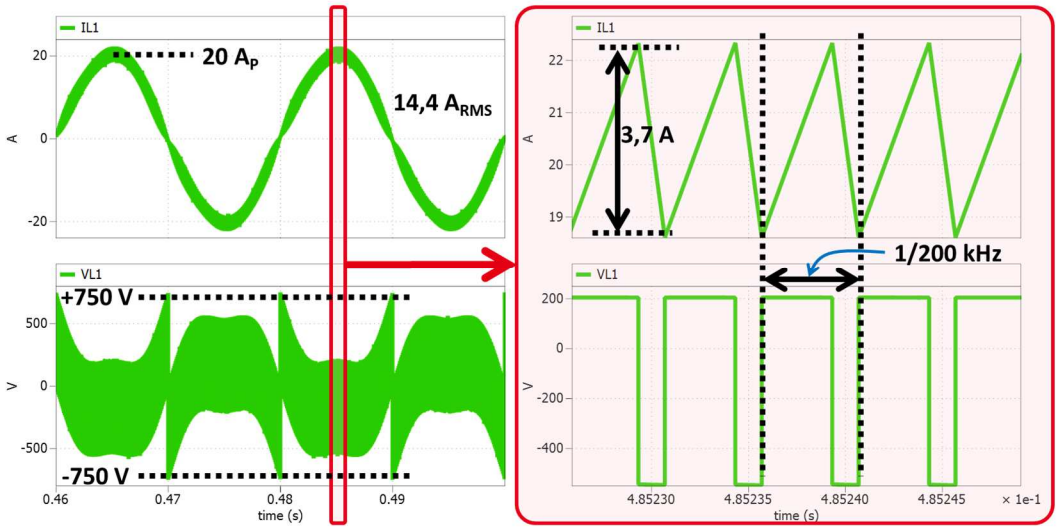

Fig. 10: Simulation results: waveforms on the output filters with twice higher working frequency

Output filters design

In this work, the GaN based 3-level flying capacitor 1500 V inverter operates with an output LCL passive filter configuration. As we can see on the simulation, in this flying-capacitor topology, the output filters operate at a double switching frequency compared to GaN power devices. That is why the magnetic materials of these filters should be able to operate at high frequency and at the same time, the associated windings should have a low AC loss in high frequency

The targeted inductance value for the larger inductive filter element is 200 µH and should be held constant during operation within a wide range of current values. This performance are obtained providing that the magnetic core works in a linear regime, i.e. the partial saturation of the core has to be avoided. The inductance design has been performed using the standard rules with large margin regarding the maximum average induction allowed in the core. A special attention has been paid to the thermal heating control of both the core and winding. The temperatures have been calculated at the nodal position over a 3D meshing by considering the core and winding losses as heat sources and the cooling by natural convection regime at boundary condition. The thermal resistance network and its numerical implementation were described in a previous work [10]. We considered two kinds of ferromagnetic material:

(i) a MnZn ferrite from TDK (N87)

(ii) a powder core from Magnetics (Koolµ60)

Commercial core geometries from the supplier catalogs have been screened, and for each material, a tradeoff has been found between the compactness and the heating. The characteristics of the designed inductors are listed in Table I.

Table I: Characteristics of the designed inductors

	Ferrite core (N87)	**Powder Core (Koolµ60)**
Core + winding volume	421 cm^3	315 cm^3
Turn number with 729 x 0.071 mm Litz wire	6	22
Gap	0.5 mm	1 mm
Iron loss	4.5 W	3 W
Winding loss	10 W	14 W

The calculated temperature maps are plotted on Fig11. It can be seen that the configuration with the Koolµ60 core is more prone to the winding heating due to a larger turn number compared to the N87 inductor. This is a consequence of the lower permeability of the powder core (µr=60) vs the ferrite one (µr = 1700).

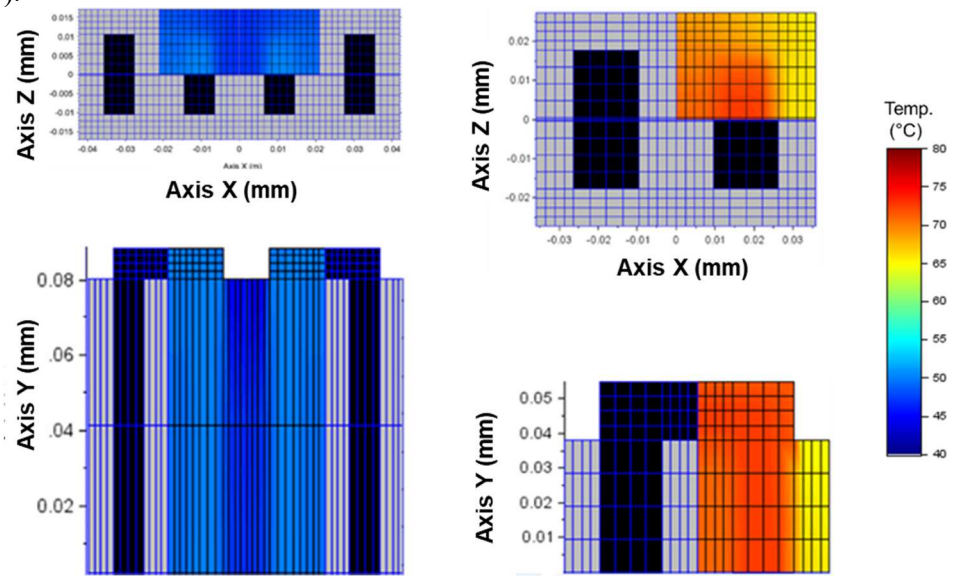

Fig. 11: Temperature maps for Ferrite (left) and Koolµ (right) solutions

In the same time, cooling of the ferrite solution was improved thanks to a larger external surface. Finally, with a maximal operating temperature of 80°C, the Koolµ60 core volume is 25 % lower than the volume of its ferrite counterpart.

Fig. 12 and Fig. 13 shows that the inductance value measured on inductors prototypes remains steady up to 40 A for the two selected materials.

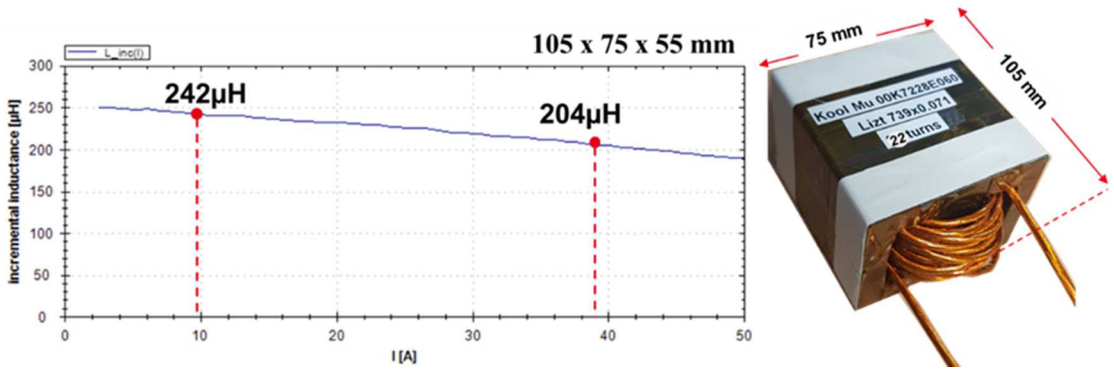

Fig. 12: Kool-Mµ based output filter with 22 turns of Litz wires: 105 x 75 x 55 mm

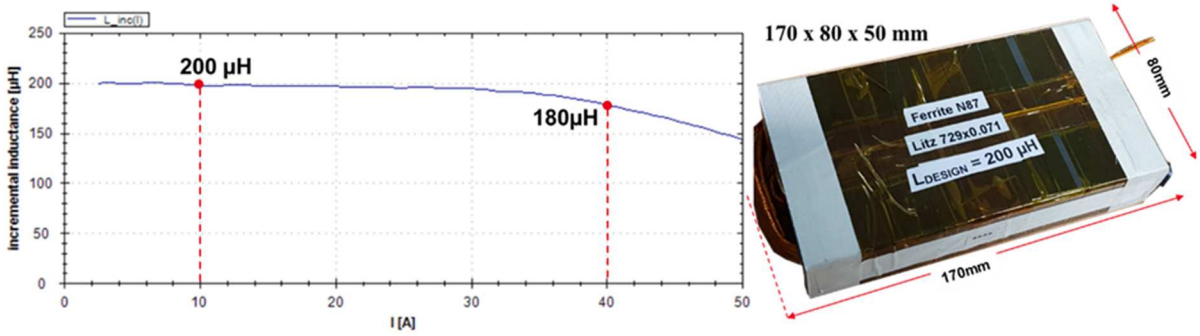

Fig. 13: Ferrite N87 based output filter with 6 turns of Litz wires: 150 x 80 x 50 mm

Experimental results on a flying capacitor inverter with GaN devices

In this part, the experimental results with GaN devices are given within the 3-level 1500 V inverter. Fig. 14 shows the schematic of the 3-phase flying-capacitor inverter on the left side where the input voltage is 1500 V_{DC} and the output is 3-phase 800 V_{AC}.

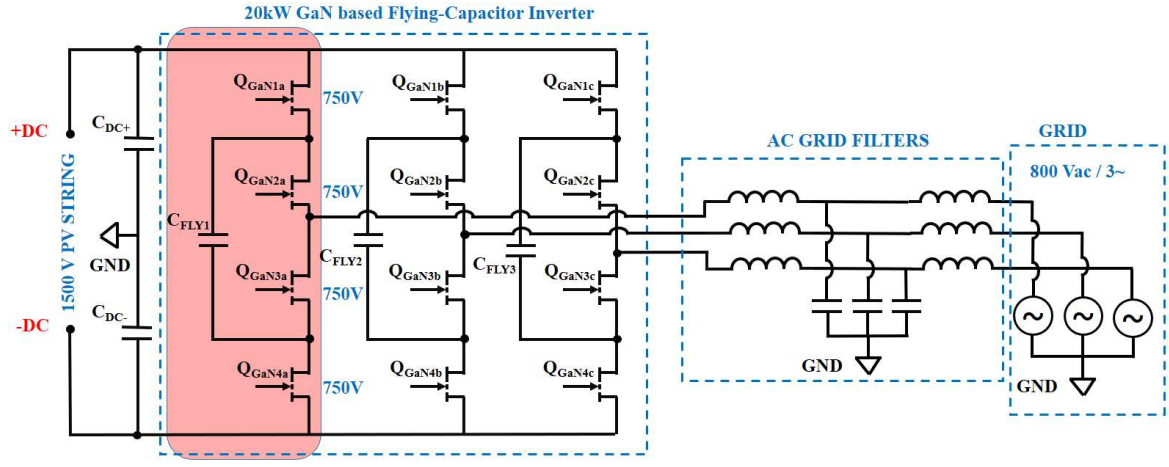

Fig. 14: Schematic of the 3-phase flying-capacitor inverter

On the right side of Fig. 13, GaN based active parts for one phase are demonstrated with GaN HEMT 1200V devices, so-called DUT2 in the previous sections, integrating gate driver Hey-1011 dedicated to GaN devices, GaN transistors are driven by V_{GS} of 0/6 V. In order to mitigate the influences of the EMI perturbations, the optical communications (optical controls and optical measurements) with an Imperix controller were implemented, and the batteries supply all the auxiliary circuits. The size of this part is 150 x 150 x 80 mm including the underneath heatsink. This is the first implementation of the GaN based Flying-capacitor inverter within this article; we call it version 1 (V1). In this implementation, we could not increase the DC bus voltage up to the nominal value; we are working on the modification of this

version for a further experiment, in particular, driving GaN HEMTs by negative base voltage to avoid the spike on the gate when the high *dv/dt* occurs.
In the middle of Fig. 15, the second version of the GaN based Flying-capacitor inverter (V2) with GaN FET 900 V; the gate drivers Si8271 with the isolated power supplies generate V_{GS} of 0/9 V. Due to high *dv/dt*, once again, this set-up could not perform at the nominal DC bus voltage. On the left side of Fig. 3, the third version of the GaN based Flying-capacitor inverter (V3) with GaN FET 900 V; the gate drivers Si8271 with the isolated power supplies generate V_{GS} of -5/14 V. To simplify the implementation, the Imperix's voltage and current sensors replace the optical onboard measures. By using this set-up, the GaN devices could perform at nominal input voltage, and generate the suitable sinusoidal output voltage for 3-phase grid of 800 V. In the designs with GaN FET 900 V, the GaN power in packaging TO-247 are between the board of the auxiliary circuits and the heatsink.

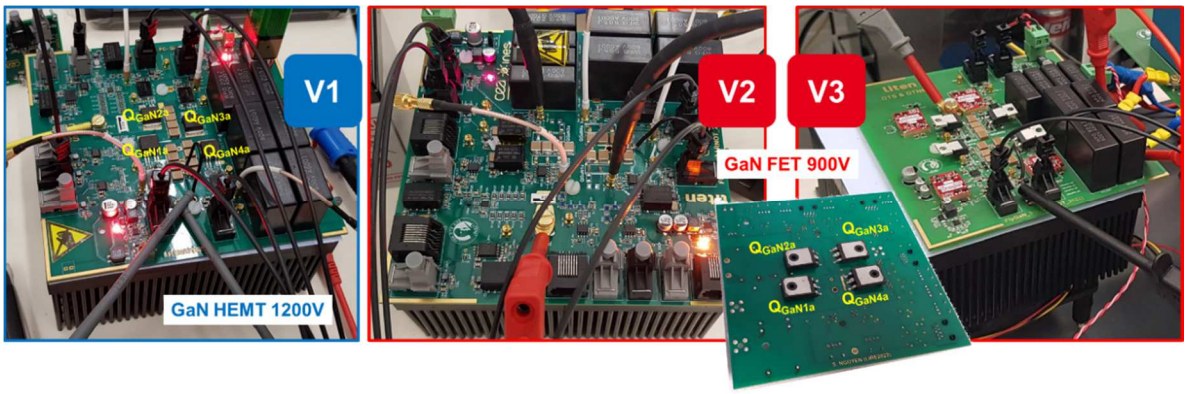

Fig. 15: Three different versions of GaN based active parts for the implementation of one-phase

For one-phase implementation in Fig. 16, bulky input capacitors (900 µF/1500 V) have been used to mitigate the 100 Hz fluctuant voltage on the input DC bus voltage, these bulky capacitors do not exist in the final 3-phase inverter. Using these high voltage GaN devices where GaN HEMT are still prototype devices for these implementations, the authors preferred to implement one-phase experiment before going further for the full implementation of the 3-phase inverter.

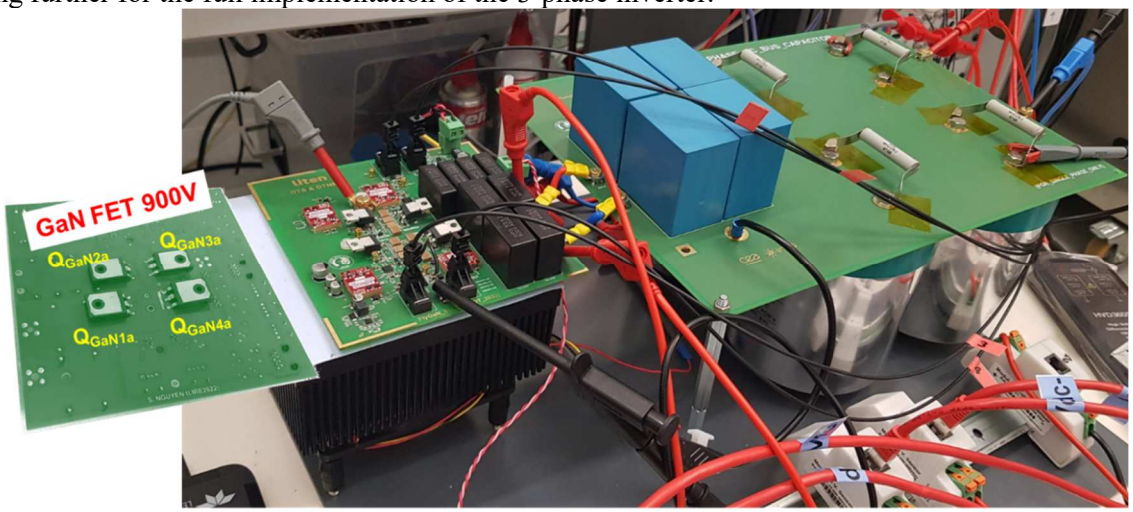

Fig. 16: Experiment of one-phase GaN FET 900V based inverter leg

Fig.17 shows the 100 kHz control signals of four GaN devices in a leg of the flying-capacitor topology, also the 3-level voltage at the middle point of the leg connected to the AC grid filter. With all the three versions of the implementations, these control signals and the 3-level voltage perform correctly at the low DC bus voltage. The differences appear at a higher DC bus voltage when the *dv/dt* becomes critical to the low threshold voltage of GaN devices.

Fig. 17: Control signals of four GaN devices in a leg and the 3-level voltage of the leg

Finally, the experimental results in the nominal DC-Bus voltage are given in the Fig. 18 where the input DC-bus voltage is 1420 V (on channel 4 – green color), the flying-capacitor voltage is approximately 710 V (channel 2 – red color). At the output on a resistive load for this experiment, the output sinusoidal RMS voltage (on channel 3 – cyan color) is 462 V_{AC}, this voltage is equal to 800 V/$\sqrt{3}$ as line to neutral value. The output RMS current is 25.6 A (on channel 1 – yellow color), where the maximum current goes through the output filter is up to 40 A. The output power in this single-phase or so-called one-phase experiment is 11.8 kW with a fan underneath the heatsink. Based on these experimental results, in the full configuration, the power of the 3-phase GaN based flying-capacitor could reach almost 36 kW.

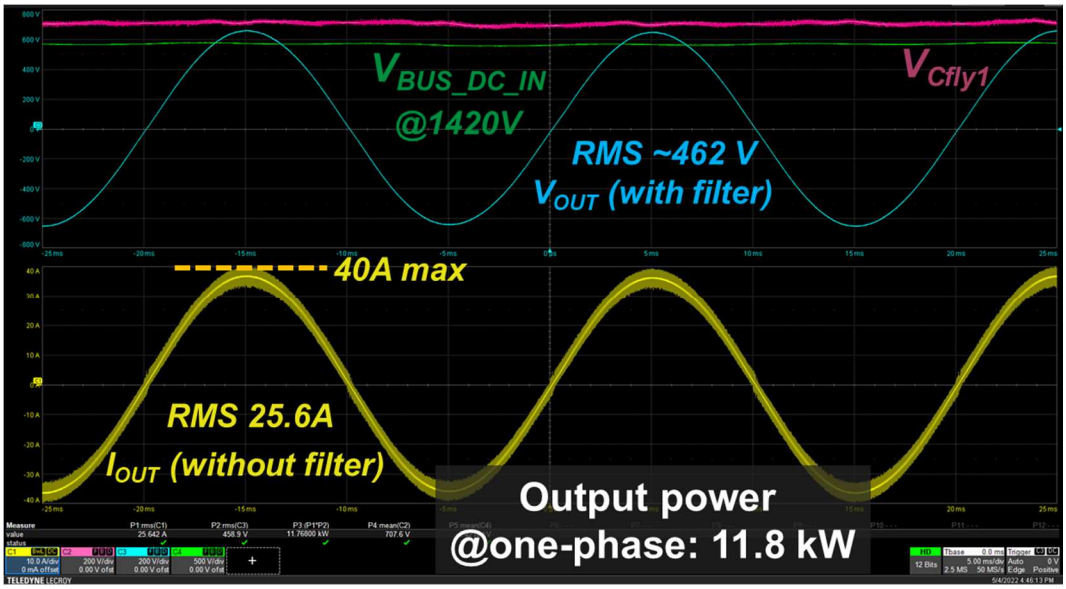

Fig. 18: Waveforms of a one-phase inverter under DC bus voltage of 1420V

Fig. 19 shows the thermal result of this one-phase inverter leg under 11.8 kW active output power, for a short duration of the experiment, the temperature on the packaging of GaN devices reach 40°C and keep increasing.

We are working to demonstrate the complete 3-phase inverter with both GaN HEMT 1200 V and GaN FET 900 V with modifications on the gate driver circuitry for GaN HEMT 1200 V, on the thickness of PCB and betterments on the thermal perspectives. The grid-tie protocols implement as our control loops for a grid-tie three-phase current source inverter [11-12]. Eventually, in this demonstration of the complete 3-phase inverter, we are going to measure the stabilized temperature on the GaN power devices and the efficiency of the inverter.

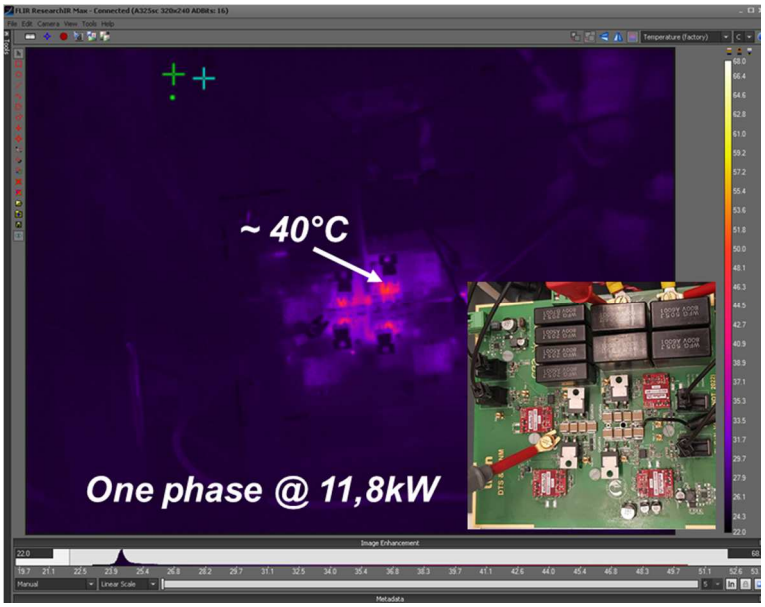

Fig. 19: Thermal image of one-phase under the output power of 11.8 kW

Conclusion

This work presents the design of a 3-level flying capacitor 1500 V_{DC} inverter with characterized GaN devices for 3-phase grid-tie applications where GaN devices perform under 750 V in steady-state operation. The static and dynamic characterizations take place to ensure the operation of the selected high voltage GaN devices in a nominal configuration. The paper include the PLECS simulations for this flying capacitor topology to identify the different working frequency of the elements in the inverter. The current and the voltage across the elements are presented in order to design the passive devices of the inverter; in particular, the output inductor filter is 3D-designed, optimized, characterized in this work. In addition, the design, the detailed characterizations of this compact GaN based flying-capacitor inverter with its dedicated output filters are given. We show several difficulties due to the GaN devices themselves and issues on the design of gate driver and their power supplies. Finally, an experiment was performed at the nominal voltage of the PV string, 1500 V. The nominal power announced is 20 kW as the power of a smart PV string [6], however the experimental characterizations show that the output power of this flying capacitor 1500 V_{DC} inverter can reach almost 36 kW. The realization of a complete 3-phase inverter is ongoing with improvements on the mechanical and thermal point-of-views.

References

[1] Yole report on Power SiC 2020: Materials, Devices and Applications, Yole 2020

[2] Yole report GaN power 2021: epitaxy, devices, applications and technology trends, Yole 2021

[3] M. Farhangi, Y-P. Siwakoti, R. Barzegarkhoo, S. Ul Hasan, D. Lu, D. Rogers “A Compact Design Using GaN Semiconductor Devices for a Flying Capacitor Five-Level Inverter” 2021 IEEE Energy Conversion Congress and Exposition (ECCE), nov 2021

[4] L-G. Alves Rodrigues, G. Perez “A 200 kW Three-level Flying Capacitor Inverter using Si/SiC based Devices for Photovoltaic Applications” PCIM Europe digital days 2021, May 2021

[5] E. Bunin (VisIC) “Performance and cost benefits of D3gaN in 3-level 800V EV inverters” PCIM Europe digital days 2021, May 2021

[6] S. Catellani, V-S. Nguyen, A. Bier, T. Delaplagne, P. Merhej, F. Bizzarri “GaN based panel-integrated, high-efficiency DC/DC optimizer for maximizing the yield of the large photovoltaic power plant” PVSEC 2022

[7] V. S. Nguyen, A. Bier, R. Escoffier, S. Catellani, J. Martin, C. Gillot “A high precision dynamic characterization bench with a current collapse measurement circuit for GaN HEMT operating at 175°C” PCIM Europe digital days 2021, May 2021

[8] K. Klein, D. E. Hoene, and D. K.-D. Lang, “Comprehensive AC Performance Analysis of Ceramic Capacitors for DC link usage,” p. 7, 2017.

[9] K. Klein, D. E. Hoene, and D. K.-D. Lang, “Power module design for utilizing of WBG switching performance,” p. 8, 2019

[10] G. Delette, U. Soupremanien and S. Loudot, "Thermal Management Design of Transformers for Dual Active Bridge Power Converters," in IEEE Transactions on Power Electronics, vol. 37, no. 7, pp. 8301-8309, July 2022

[11] A. Bier: Three-phase grid-tied current-source inverter sizing and control for photovoltaic application, SPEEDAM, June 2016

[12] A.Bier, V-S. Nguyen, S. Catellani, J. Martin " Control of a single-phase grid-tied GaN based solar micro-inverter" EPE 2020 (22nd European Conference on Power Electronics and Applications, EPE’20 ECCE Europe), Sept 2020